Solar Energy Materials & Solar Cells 207 (2020) 110357

Contents lists available at ScienceDirect

Solar Energy Materials and Solar Cells

journal homepage: http://www.elsevier.com/locate/solmat

Double-sided TOPCon solar cells on textured wafer with ALD SiO_x layer

Mickaël Lozac'h *, Shota Nunomura **, Koji Matsubara

Research Center for Photovoltaics, National Institute of Advanced Industrial Science and Technology (AIST), 1-1-1 Umezono, Tsukuba, 305-8568, Japan

ARTICLE INFO

Keywords:
Surface passivation
Polycrystalline silicon (poly-Si)
Tunnel oxide passivated contact (TOPCon)
Silicon oxide (SiO_x)
Atomic layer deposition (ALD)

ABSTRACT

Double-sided, front and rear, tunnel oxide passivated contact (TOPCon) of crystalline silicon (c-Si) solar cells on textured wafer is presented. The double-sided TOPCon structure is composed of (p) poly-Si/SiO_x/(n) c-Si/SiO_x/(n) poly-Si, where the silicon oxide (SiO_x) layer is formed by atomic layer deposition (ALD). With a 0.6 ± 0.1 nm-thick SiO_x layer, an 18.8 %-efficiency solar cell is fabricated, where an excellent short circuit current above 39 mA/cm^2 is confirmed for a front grid structure. The solar cell performance is improved by optimizing the boron and hydrogen diffusion profiles near the p-side SiO_x/c-Si interface.

1. Introduction

The tunnel oxide passivated contact (TOPCon) of crystalline silicon (c-Si) solar cells gains much attention recently since it exhibits a high photoconversion efficiency over 25% with a relatively simple structure using front and rear ohmic contacts, easily transferable at industrial scale [1]. This TOPCon, also called poly-Si, SIPOS [2], or POLO-IBC [3,4], is composed of a doped polycrystalline Si (poly-Si)/silicon oxide (SiO_x) stack. The thickness of the SiO_x layer should be below ~1.5 nm to allow the tunneling transport of photocarriers [5]. The ultrathin SiO_x layer is prepared by wet chemical oxide [5,6], dry oxide [3], or UV-O_3 [7], which yields an excellent passivation for the polished c-Si surface. However such passivation is strongly degraded for the textured surfaces [6,8]. Besides, the passivation is known to be weakened by the (p) poly-Si/SiO_x stack, compared with the (n) poly-Si/SiO_x stack for n-type Si wafer [8–18]. Therefore, the surface passivation of a textured c-Si wafer for the p-side is crucial for further development of high-efficiency TOPCon solar cells. Recent works already mention the use of front and rear TOPCon solar cells [6,12,15,19], some have only the front side textured used with the (n) stack [6,19].

The fabrication of TOPCon solar cell involves a high temperature (high-*T*) annealing about 850 °C, where the dopants diffuse from the doped poly-Si layer to the SiO_x interface creating a field effect passivation and also inside the c-Si wafer generating a junction. The high-*T* annealing also induces the effusion of hydrogen from the SiO_x/c-Si interface, and thus a hydrogenation step is necessary to terminate chemically the dangling bonds [5]. The dopant diffusion and hydrogenation phenomena are highly dependent on the SiO_x thickness, the dopant concentration in the poly-Si layer [20], the hydrogenation method, and the surface morphology, which complicate the process optimization of TOPCon solar cells.

In this study, double-sided, front (p) and rear (n), TOPCon solar cells on textured wafer are presented. This structure consists of (p) poly-Si/SiO_x/(n) c-Si/SiO_x/(n) poly-Si. The SiO_x layer is formed by atomic layer deposition (ALD), which yields excellent conformal coverage over the textured surface. The ALD technique also yields the thickness control of the SiO_x layer at atomic level [10]. Here, we particularly concentrate on the surface passivation of the p-side over the textured c-Si. The boron and hydrogen distributions near the (p) poly-Si/SiO_x stack are controlled by the boron doping rate in the precursor film of hydrogenated amorphous silicon (a-Si:H). The solar cell characteristics are discussed in term of boron and hydrogen distributions, measured by secondary ion mass spectrometry (SIMS).

2. Experimental

2.1. Wafer texturing and cleaning

Floating zone (FZ) silicon wafers (n-type phosphorus-doped, 1–5 Ωcm, 280 μm-thick, ⟨100⟩- oriented, and polished double sides) are textured by KOH chemical etching at 80 °C for 15 min, removing about 10 μm on front and rear surfaces cumulated [21]. Then, the wafers are cleaned by our standard cleaning process [22] to remove the native oxide and the impurities on surface. This process consists of (i) native

* Corresponding author.
** Corresponding author.
E-mail addresses: mickael.lozach@aist.go.jp (M. Lozac'h), s.nunomura@aist.go.jp (S. Nunomura).

https://doi.org/10.1016/j.solmat.2019.110357
Received 19 November 2019; Received in revised form 6 December 2019; Accepted 12 December 2019
Available online 17 December 2019

oxide removal and chemical oxide growth by a self-heated solution at 75 °C for 15 min (H_2SO_4:H_2O_2 ratio 4:1), (ii) an oxide etching for 2 min (HF:HCl:H_2O ratio 1:1:20), (iii) an oxide growth for 15 min (HCl:H_2O_2:H_2O ratio 1:1:5), then (iv) a diluted HF (DHF) solution for 30 s (HF:H_2O ratio 1:20) to remove the oxide layer and to saturate the surface termination by H atoms. Between each process, the cleaned wafers are transferred into a vacuum box to reduce the oxidation and contamination. The H-termination surface of silicon wafer is stable up to 30 min under ambient air [23,24].

2.2. Silicon oxide, a-Si:H deposition, and post annealing

The ultrathin SiO_x layer is deposited by means of plasma assisted ALD (Oxford Instruments FlexAL® system). The deposition temperature is set at 300 °C for the full ALD process. The tris(dimethylamino)silane (3DMAS) precursor is used as a silicon source. An oxygen (O_2) plasma is used as an oxygen source, generated by an inductively coupled plasma (ICP) with 13.56 MHz radio frequency (RF) power of 250 W at an O_2 pressure of 15 mTorr for 3 s. The thicknesses are controlled by adjusting the number of ALD cycles and the sources exposure time (3DMAS and O_2 plasma). For polished surface wafers, the SiO_x thickness is monitored by spectroscopic ellipsometry (SE) in situ using a Cauchy model.

The c-Si wafers are then transferred into plasma-enhanced chemical vapor deposition (PECVD) system in a down-flow configuration for the deposition of a-Si:H precursor films. Here, the p-type precursor film is composed of the (p)/(i) a-Si:H stack, where the boron concentration in (p) a-Si:H layer is varied. This (p)/(i) a-Si:H stack allows us to control the dopant concentration and distribution after the high-*T* annealing, as described in the next section. For the n-type poly-Si precursor, the phosphorous doped (n) a-Si:H is used without (i) a-Si:H layer. The p- and n-type a-Si:H are deposited at 140 °C with a mixture of SiH_4, H_2 and B_2H_6 flows, and SiH_4, H_2 and PH_3 flows, respectively. The B_2H_6 flow is changed in a range of 5–200 sccm to control the boron doping. The i-type a-Si:H is deposited at 165 °C with a mixture of SiH_4 and H_2 [25]. The thicknesses of these a-Si:H layers are determined from SE assuming a Tauc-Lorentz model.

Next, the samples are annealed in a furnace at 820 °C for 1 h under vacuum condition. The temperature ramps are set as low as 100 °C/h for the annealing and the cooling down to prevent blistering effect on surface [26,27].

2.3. Hydrogen plasma treatment

During the high-*T* annealing step, the hydrogen atoms effuse from the material, resulting in a poor passivation property of the poly-Si/SiO_x stack [10]. Thus, a hydrogenation step is necessary to terminate the defects such as dangling bonds in the material [28]. In this study, the hydrogenation is performed by hydrogen plasma treatment (HPT) in capacitively-coupled discharge at 300 °C for 1 min [29,30]. The pressure inside the chamber is set at 0.5 Torr, the power density at 60 mW/cm^2, and the frequency at 85 MHz. The distance between the electrodes in a parallel-plate configuration is about 2 cm.

2.4. Characterization of the passivation

The effective lifetime (τ_{eff}) of minority carriers, the implied open-circuit voltage (iV_{oc}), and the saturation current density (J_0), are measured on symmetric structures and non-symmetric structures on polished and textured c-Si surfaces. The passivation is characterized at room temperature by using the quasi-steady-state photoconductance method (QSSPC, Sinton WTC-120) [31]. The passivation property is evaluated by the effective lifetime of minority carriers at an injection level of 1×10^{15} cm^{-3}. A high τ_{eff} reflects a high-quality passivation.

2.5. Solar cell structures

The solar cell structure fabricated in this study is Ag (3.6 μm)/ITO (70 nm)/(p) poly-Si (22 ± 1 nm)/SiO_x (0.6 ± 0.1 nm)/(n) c-Si (~270 μm)/SiO_x (0.6 ± 0.1 nm)/(n) poly-Si (22 ± 1 nm)/ITO (70 nm)/Ag (0.7 μm), as shown in Fig. 2b. The cell size is ~1.0 × 1.0 cm^2 over a 5.0 × 5.0 cm^2 substrate wafer. As described in the introductory part, the (p) poly-Si/SiO_x stack plays an important role in the passivation property. So, the dopant concentration in (p) poly-Si is controlled by the precursor film of the (p)/(i) a-Si:H stack, where the boron concentration is changed, as described above. The double-sided TOPCon structure as deposited is (p) a-Si:H (2 ± 1 nm)/(i) a-Si:H (20 ± 1 nm)/SiO_x (0.6 ± 0.1 nm)/c-Si/SiO_x (0.6 ± 0.1 nm)/(n) a-Si:H (22 ± 1 nm). After high-*T* annealing at 820 °C, the (p)/(i) a-Si:H stack is converted to a single (p) poly-Si layer with the same thickness. The (p) poly-Si layer is about 22 nm to minimize the ITO sputtering damage [32]. Hereafter, we denoted the (p) and (n) poly-Si/SiO_x stacks as (p) and (n) stacks, respectively.

After high-*T* annealing and HPT steps, ITO films are deposited by sputtering technique at the front and rear surfaces as an anti-reflective and conductive coating. A low temperature post annealing step is widely used to recover from the ITO sputtering damage [12,33,34]. In this study, a low temperature post annealing is performed at 160 °C for 2 h. Then, the front and rear Ag contacts are deposited.

The current-voltage (I–V) characteristics of the solar cells are performed under the standard AM 1.5G (100 mW/cm^2) irradiance. The illuminated area, used for the measurement of the short-circuit current (J_{sc}) and thus the photoconversion efficiency, is measured at 1.045 cm^2, which includes the active area (1.017 cm^2) and the grid shadowing (0.028 cm^2). The contact resistivity ρ_c with the (p) poly-Si layer is measured by the transmission line method (TLM) on a specific front line patterned beside the solar cells from the same c-Si wafer.

3. Experimental results

3.1. Conformal coverage by ALD

The transmission electron microscope (TEM) images in Fig. 1 present the principal advantage of the plasma assisted ALD technique: the conformal thicknesses of SiO_x deposited on both polished and textured surfaces are excellent with no thickness variation. Fig. 1a and Fig. 1b correspond to TEM images of (p) a-Si:H/SiO_x stack as-deposited and after thermal annealing at high-*T*, respectively, deposited on polished c-Si surfaces. For the samples on polished surfaces, the SiO_x layer is prepared using 3 ALD cycles with a source time exposure of 3 s corresponding to a thickness measured at 1.0 ± 0.1 nm. After high-*T* annealing, Fig. 1b underlines clearly the poly-crystalline (poly-Si) nature with some areas presenting well-organized atomic plans and some other areas remaining amorphous. Figs. 1c and **d** present the diffraction patterns of the poly-Si compared to the one of the bulk c-Si, the poly-Si does not present a clear organization such as the bulk, which confirms the "not completely" crystallized nature of the poly-Si layer [18]. Fig. 1e and Fig. 1f show the (p) stack after high-*T* annealing on textured c-Si surfaces. Here, the main advantage of the ALD technique is underlined with a uniform SiO_x layer even at the bottom of the textured valley (Fig. 1e). The magnification (Fig. 1f) underlines also a poly-Si nature with random and well-oriented atomic plans. For this specific sample, the SiO_x layer is prepared using 3 ALD cycles with a source time exposure of 10 s corresponding to a thickness measured at 2.4 ± 0.1 nm. The deposition conditions for the (p) a-Si:H layer are identical for the polished and textured c-Si, which results in a well-known ~ 30% thinner layer for the textured samples. A top view of the textured sample is also presented that confirms the micron-sized pyramid texture (Fig. 1g).

3.2. Solar cells performance depending on the boron concentration

Fig. 2a shows the solar cell characteristics as a function of the B_2H_6

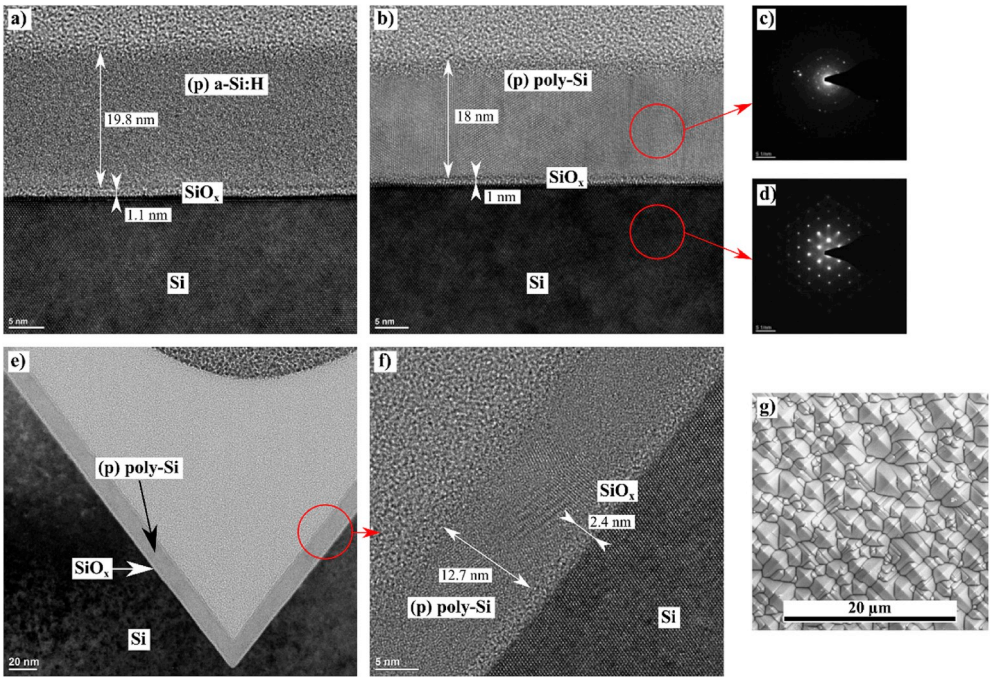

Fig. 1. TEM images of **a)** (p) a-Si:H/SiO_x on polished surface as deposited, **b)** (p) poly-Si/SiO_x on polished surface after high-*T* annealing. Diffraction patterns of **c)** the (p) poly-Si compared to **d)** the bulk-Si by nano beam diffraction (NBD). TEM images of **e)** (p) poly-Si/SiO_x on textured surface after high-*T* annealing, **f)** magnification of **e)**. **g)** Plane view of the textured surface.

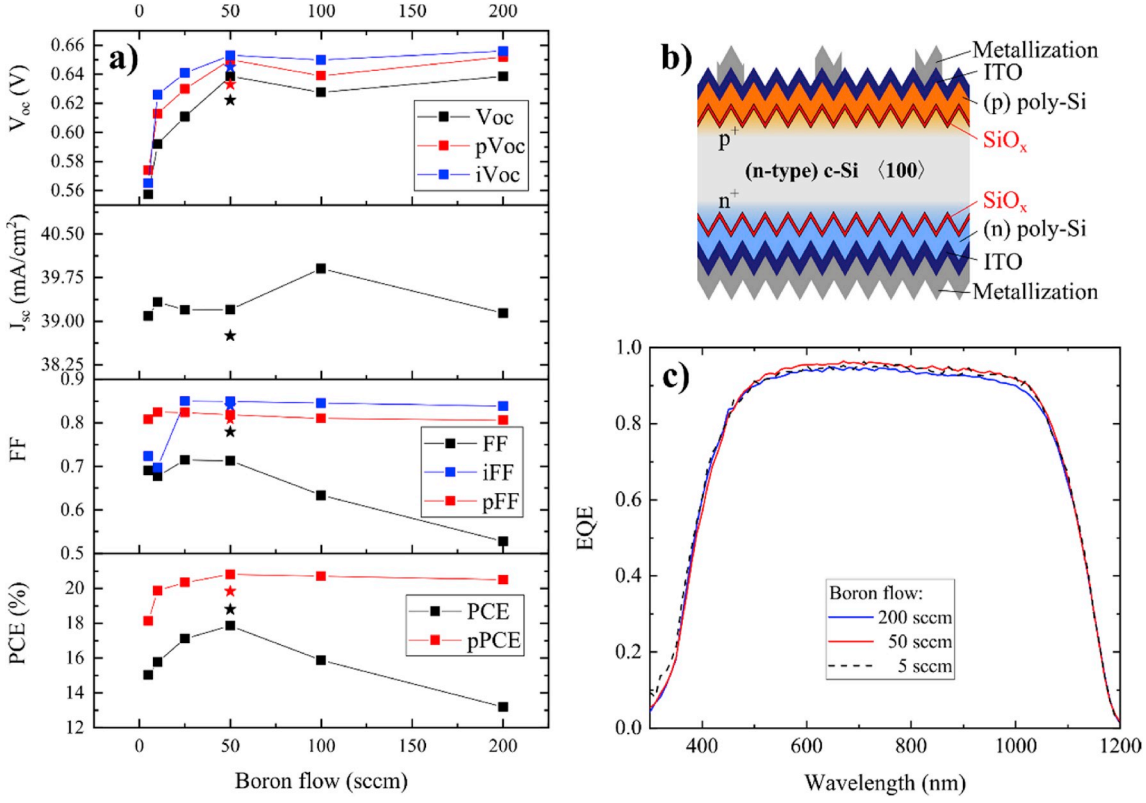

Fig. 2. a) Solar cell characteristics as a function of the B_2H_6 flow for (p) poly-Si (22 ± 1 nm)/SiO_x/c-Si/SiO_x/(n) poly-Si (22 ± 1 nm) structure. **b)** Illustration of the solar cell structure. **c)** The external quantum efficiency (EQE) is shown for 3 B_2H_6 flows condition at 5 sccm, 50 sccm, and 200 sccm.

flow during the deposition of the (p) a-Si:H precursor layer. For a B_2H_6 flow between 50 sccm and 200 sccm, the V_{oc}, the pseudo V_{oc} (pV_{oc}), and the implied V_{oc} (iV_{oc}) are almost constant about 638 mV, 650 mV and 655 mV, respectively. On the other hand, these parameters quickly dropped once the B_2H_6 flow is reduced below 50 sccm, which is also observed in other work using trimethylboron (TMB) as dopant flow [35]. The short-circuit current J_{sc} is measured above 39 mA/cm^2 at any flow. The implied fill factor (iFF) is about 0.84 for a B_2H_6 flow at 200

sccm, about 0.85 at 50 sccm, and drop quickly for lower flow, while the measured FF has a maximum about 0.71 at 50 sccm and drop for lower and higher flows. So, the photoconversion efficiency (PCE) displays a maximum at 17.8% for a B_2H_6 flow at 50 sccm. The corresponding pseudo PCE (pPCE) reaches 20.8% under the optimized condition.

The solar cell performance is improved by the insertion of an additional DHF step of 30 s prior to the ITO sputtering, shown in Fig. 2a (star points). This DHF step is used to etch a possible oxide layer and/or defective layer at the surface of the poly-Si. The iFF and pFF are measured at 0.84 and 0.81, and the FF reaches 0.78. This yields an improvement of the PCE at 18.8% even if the pPCE decreases about 20.1% due to the iV_{oc}, pV_{oc}, and V_{oc} that slightly decrease about 645 mV, 630 mV, and 622 mV, respectively.

The external quantum efficiencies (EQE) are presented in Fig. 2c for the solar cells with B_2H_6 flows at 5 sccm, 50 sccm, and 200 sccm. It is clearly shown that the EQE spectra exhibit an excellent response over a wide wavelength range from 400 nm to 1100 nm. For the EQE at 5 sccm, the short wavelength responses from 480 nm to 800 nm slightly decreases compared to the optimized condition at 50 sccm. The EQE at 200 sccm is lower over a large spectral range from 480 nm up to 1050 nm compared to the optimized condition at 50 sccm.

3.3. SIMS analysis

The depth profile of the boron (B) and the hydrogen (H) are analyzed by secondary ion mass spectrometry (SIMS). These depth profiles are presented after high-*T* and HPT steps. For comparison, two reference samples are prepared; one is the (p) a-Si:H (22 nm)/SiO_x stack as the "as-deposited" reference, and the other one is the (p) poly-Si (22 nm)/SiO_x stack as the "high-*T* annealed" reference, both without the (i) a-Si:H precursor layer.

Fig. 3a presents the depth profiles of the boron concentration. The as-deposited (p) a-Si:H reference profile, denoted by the (p) a-Si:H (22 nm) curve, shows no boron diffusion into c-Si, where the boron concentration is measured at 10^{21} at/cm^3 for the first 22 nm and steeply decreases to 10^{16} at/cm^3 at 40 nm depth. After high-*T* annealing and HPT, for the heavy doped (p) poly-Si (22 nm)/SiO_x reference, boron accumulates at the surface and at the SiO_x interface [13,15], with a peak at 2.8×10^{21} at/cm^3, and the boron concentration diffused inside c-Si is measured about 2×10^{19} at/cm^3 with a junction depth about 150 nm, as shown by the (p) poly-Si (22 nm) curve. The insertion of (i) a-Si:H layer (20 nm) with a thin (p) a-Si:H layer (2 nm) for the formation of (p) poly-Si significantly decreases the boron accumulation at the interface with SiO_x and also the junction depth. Only the front stack precursors (p) a-Si:H (2 ± 1 nm)/(i) a-Si:H (20 ± 1 nm)/SiO_x (0.6 ± 0.1 nm) are used for the solar cell devices. For B_2H_6 flows at 200 sccm, 50 sccm, and 5 sccm, the boron concentrations at SiO_x interface are measured at 1.8×10^{20} at/cm^3, 1.3×10^{20} at/cm^3, and 1.8×10^{19} at/cm^3, respectively, with a junction depth about 120 nm, 100 nm, and 60 nm. It should be emphasized that a high concentration of boron is detected at the surface of the (p) poly-Si about 5×10^{21} at/cm^3 for the sample at 200 sccm.

Fig. 3b shows the depth profiles of the H concentration. The peaks of H concentration, i.e., the H accumulation, appear for the as-deposited films at the surface and at the SiO_x interface about 10^{22} at/cm^3. Within the (p) a-Si:H film, H is measured about 8×10^{21} at/cm^3. For all annealed and HPT samples, the remaining H is accumulated at the surface and at the SiO_x interface. The H concentration at the SiO_x interface decreases by one order of magnitude, showing about 1.2×10^{21} at/cm^3 - 2.0×10^{21} at/cm^3, for these three cases.

For the heavy doped (p) stack, the H concentration peak at SiO_x interface decreases by two orders of magnitude about 4.0×10^{20} at/cm^3. Due to the effusion during the high-*T* annealing, the H concentration inside the (p) poly films is much lower: the H concentration is measured at 1×10^{20} at/cm^3, 1.5×10^{20} at/cm^3, and 4×10^{20} at/cm^3, for (p) poly-Si using 200 sccm, 50 sccm, and 5 sccm, respectively, and at 4×10^{19} at/cm^3, one order of magnitude lower, for the heavy doped (p) poly-Si film.

4. Discussions

The advantages of the ALD technique are well underlined in Fig. 1 with an excellent conformal SiO_x layer, even at the valleys of the texturization. Interestingly, we do not observe any pinhole in the TEM images, which can suggest a current flow via tunneling effect through the SiO_x layer [36]. Another advantage of the ALD technique concerns the precise control of the film thickness at atomic scale, which is necessary to reach a good passivation property. Indeed, we observe that an ultrathin SiO_x deposited with only one ALD cycle and a source exposure time below 10 s is necessary to reach τ_{eff} above 1 ms for (n) stack symmetric structure on textured surface.

The solar cell characteristics present a clear dependency on the boron concentration with an optimum at 50 sccm, where the photoconversion efficiency is improved (Fig. 2a). For a B_2H_6 flow lower than 50 sccm, the PCE decreases due to a voltage loss in V_{oc}, pV_{oc}, and iV_{oc}. The pV_{oc} is consistently slightly lower than the iV_{oc}, likely due to the additional passivation losses induced by the ITO and Ag sputtering processes required to finish the cell fabrication [37], and the measured V_{oc} of finished cells is lower than the pV_{oc} due to the series resistance effect [38]. The losses in iV_{oc}, pV_{oc}, and V_{oc} are attributed to the low boron concentration for the p-n junction [35]. As observed in Fig. 3a, the boron concentration profile inside the c-Si from the (p) stack at 5 sccm is below 6×10^{17} at/cm^3 with a junction depth about 70 nm. Such weak p-n junction is not sufficient for the Fermi level splitting resulting in poor

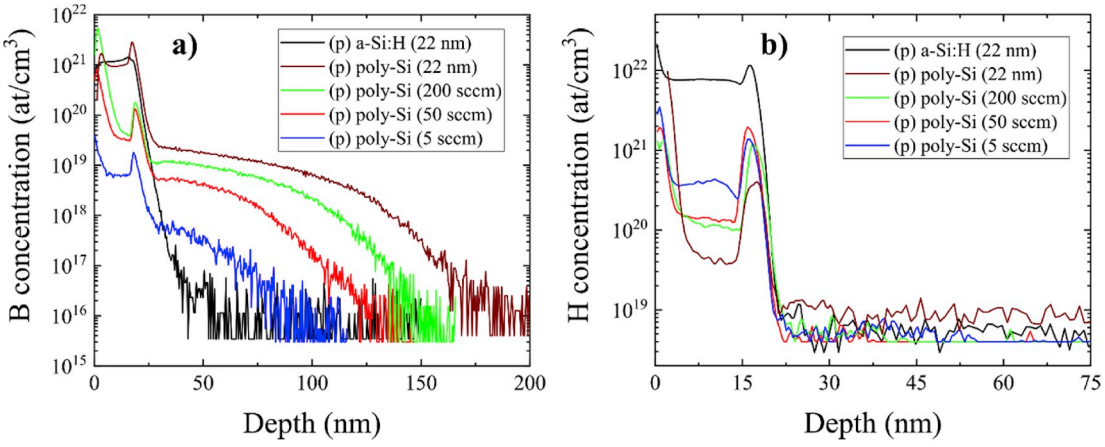

Fig. 3. SIMS profiles of **a)** the boron (B) concentration and **b)** the hydrogen (H) concentration for the front structures with different B_2H_6 flows denoted (p) poly-Si 5 sccm, 50 sccm, and 200 sccm. For references, the heavy doped (p) a-Si:H as-deposited, and (p) poly-Si are also shown. The thickness of p-layer is 22 ± 1 nm for all.

iV_{oc}. Thus, a heavier doping concentration is necessary to increase the PCE. The optimum profile in our study for the (p) stack at 50 sccm has a boron concentration inside the c-Si about 5×10^{18} at/cm^3 and a junction depth about 100 nm. For B_2H_6 flows stronger than 50 sccm, the PCE decreases due to the FF (Fig. 2a). Here also, the pseudo FF (pFF) is consistently slightly lower than the implied FF (iFF) because of the additional passivation losses induced by the ITO and Ag sputtering processes [37]. At 200 sccm, the FF strongly decreases to 0.53 while iFF and pFF remain at 0.84 and 0.81, respectively. This suggests a problem related to the series resistance, and thus the ohmic contacts. Regarding the depth profile of the B_2H_6 flow at 200 sccm (Fig. 3a), a very high boron concentration at 5×10^{21} at/cm^3 is measured, higher that the limit of solubility into a silicon matrix [39], which can suggest the presence of a defective layer that can increase the series resistance.

The FF of the fabricated solar cells are still relatively low at 0.71 for the optimized B_2H_6 flow. Thus, a DHF of 30 s is performed prior to the ITO deposition to remove the possible defective layer. The solar cell property with DHF step underlines a clear improvement of the FF at 0.78 with an enhanced PCE at 18.8% (Fig. 2a). Transmission line measurements (TLM) for the front contact with (p) poly-Si layer shows a contact resistance ρ_c at 3 Ωcm^2 for solar cell structure without DHF step, and 0.9 Ωcm^2 with DHF step. Thus, the DHF step is clearly beneficial to reduce ρ_c. It is worth noting that such DHF step may also decrease the iV_{oc}, pV_{oc}, and V_{oc} about 10 mV and consequently the pPCE is measured at 20.1%. The recombination current density prefactor J_0 for our best cells is measured at 298 fA/cm^2 by QSSPC at high injection level [40]. The PCE of 18.8% for double TOPCon-type solar cell structure on textured surfaces is plotted in Fig. 4 from J. Melskens et al. [41], with ρ_c as a function of J_0 from various c-Si solar cell concepts.

The advantages of such structure is underlined with a high J_{sc} measured above 39 mA/cm^2 considering a front contact structure and the grid shadow, with the EQE showing excellent response at short and long wavelengths (Fig. 2c). Indeed, the EQE at short wavelengths at 500 nm is excellent compared to conventional heterojunction solar cells using a (p) a-Si:H layer [42]. The EQE at 5 sccm has a lower response from 480 nm to 800 nm than the optimized condition due to the weak junction, while the EQE at 200 sccm underlines a loss for broader spectra from 480 nm to 1050 nm due to a stronger parasitic absorption within the (p) poly-Si layer.

Concerning the SIMS measurements, the boron is more soluble in the SiO_x than in the Si, making a concentration peak at the (p) poly-Si surface and at the SiO_x interface [43]. Interestingly, the insertion of a (i) layer is beneficial not only to decrease the diffusion profile of the boron dopant, but also to decrease the H effusion from the SiO_x interface and from the (p) poly-Si. Moreover, the H concentration inside the (p) poly-Si layers is decreasing with higher B_2H_6 flow. The concentration of H remains one order of magnitude higher at SiO_x interface about 2.0×10^{21} at/cm^3 and inside the (p) poly-Si layer about 1.5×10^{20} at/cm^3 for the best condition, enhancing the implied open circuit iV_{oc} at 655 mV (Fig. 2a). It is known that the accumulation of H concentration at the SiO_x interface enables higher iV_{oc} values [44]. Other group also reported a hydrogen and deuterium accumulation at the SiO_x interface about the same order at 10^{21} at/cm^3 at the SiO_x interface in (p) stack, with a H concentration within the (p) poly-Si layer about 10^{21} at/cm^3 enabling an iV_{oc} about 712 mV on polished surface [45]. For the front and rear TOPCon-type structure on double side textured surface, a PCE of 21.4% seems achievable by increasing the amount of H within the (p) stack targeting a V_{oc} at 700 mV with measured J_{sc} at 39.2 mA/cm^2 and FF at 0.78. Furthermore, such structure uses only one high thermal annealing step with standard front and rear ohmic contact that could be easily transferable at industrial scale.

5. Summary

The photovoltaic performances of a double-sided, front (p) and rear (n), TOPCon solar cell using textured wafer are presented. The ultrathin

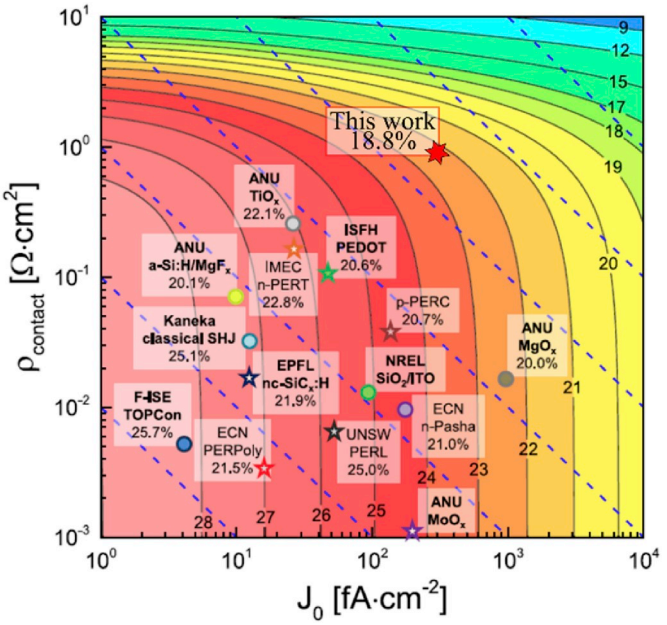

Fig. 4. Figure from J. Melskens et al. [41] with the recombination current density prefactor (J_0) and the contact resistivity ($\rho_{contact}$) for various c-Si solar cell concepts. Our best result (PCE of 18.8%) using the double-sided, front (p) and rear (n), TOPCon structure on textured c-Si wafer is plotted by red star. (For interpretation of the references to colour in this figure legend, the reader is referred to the Web version of this article.)

SiO_x layer is deposited by ALD to keep an excellent conformal thickness on textured surface. The photoconversion efficiency reaches 18.8% with a short circuit current above 39 mA/cm^2 for a front grid structure, and a fill factor at 0.78. An optimized boron concentration for the front (p) stack has been underlined with a boron concentration about 1.3×10^{20} at/cm^3 at the SiO_x interface and a junction depth about 100 nm by SIMS measurements. The boron diffusion is controlled by the precursor (p)/(i) a-Si:H stack. The H concentration at the SiO_x/c-Si interface is a key to the Si surface passivation. For the 18.8% efficiency cell, it is about 2×10^{21} at/cm^3, improving the implied open circuit to 655 mV.

We underline that the use of higher B_2H_6 flow presents a defective layer at the surface of the (p) stack generating series resistance. A DHF step prior to the ITO sputtering increases the fill factor to 0.78 by decreasing the contact resistance below 1 Ωcm^2.

Authors contribution statements

The experiment and analysis were performed by M. L. The manuscript is prepared by M.L. and S. N. The research is managed by S.N and K. M.

Declaration of competing interest

The authors declare that they have no known competing financial interests or personal relationships that could have appeared to influence the work reported in this paper.

Acknowledgements

The authors acknowledge Aiko Sato, Toshiki Oku, and Yoshiki Sato for their technical support and Takuya Matsui and Leonard Tutsch for discussions. We are grateful to Masashi Yamazaki for his expertise on ALD system. This work was supported by New Energy and Industrial Technology Development Organization (NEDO) and JSPS KAKENHI (18K03603). The ALD process was performed at the AIST Nano-Processing Facility, supported by "Nanotechnology Platform Program"

of the Ministry of Education, Culture, Sports, Science and Technology (MEXT), Japan.

Appendix A. Supplementary data

Supplementary data to this article can be found online at https://doi.org/10.1016/j.solmat.2019.110357.

References

[1] A. Richter, J. Benick, R. Müller, F. Feldmann, C. Reichel, M. Hermle, et al., Tunnel oxide passivating electron contacts as full-area rear emitter of high-efficiency p-type silicon solar cells, Prog. Photovolt. Res. Appl. 26 (2018) 579–586, https://doi.org/10.1002/pip.2960.

[2] E. Yablonovitch, T. Gmitter, R.M. Swanson, Y.H. Kwark, A 720 mV open circuit voltage SiOx:c-Si:SiOx double heterostructure solar cell, Appl. Phys. Lett. 47 (1985) 1211–1213, https://doi.org/10.1063/1.96331.

[3] F. Haase, C. Hollemann, S. Schäfer, A. Merkle, M. Rienäcker, J. Krügener, et al., Laser contact openings for local poly-Si-metal contacts enabling 26.1%-efficient POLO-IBC solar cells, Sol. Energy Mater. Sol. Cells 186 (2018) 184–193, https://doi.org/10.1016/j.solmat.2018.06.020.

[4] S. Schäfer, F. Haase, C. Hollemann, J. Hensen, J. Krügener, R. Brendel, et al., 26%-Efficient and 2 cm narrow interdigitated back contact silicon solar cells with passivated slits on two edges, Sol. Energy Mater. Sol. Cells 200 (2019), https://doi.org/10.1016/j.solmat.2019.110021, 110021.

[5] F. Feldmann, M. Bivour, C. Reichel, H. Steinkemper, M. Hermle, S.W. Glunz, Tunnel oxide passivated contacts as an alternative to partial rear contacts, Sol. Energy Mater. Sol. Cells 131 (2014) 46–50, https://doi.org/10.1016/j.solmat.2014.06.015.

[6] A. Ingenito, G. Nogay, J. Stuckelberger, P. Wyss, L. Gnocchi, C. Allebe, et al., Phosphorous-doped silicon carbide as front-side full-area passivating contact for double-side contacted c-Si solar cells, IEEE J. Photovoltaics 9 (2019) 346–354, https://doi.org/10.1109/JPHOTOV.2018.2886234.

[7] A. Moldovan, F. Feldmann, K. Kaufmann, S. Richter, M. Werner, C. Hagendorf, et al., Tunnel oxide passivated carrier-selective contacts based on ultra-thin SiO2 layers grown by photo-oxidation or wet-chemical oxidation in ozonized water, Sol. Energy Mater. Sol. Cells 142 (2015) 123–127, https://doi.org/10.1109/PVSC.2015.7356144.

[8] Y. Larionova, M. Turcu, S. Reiter, R. Brendel, D. Tetzlaff, J. Krügener, et al., On the recombination behavior of p+-type polysilicon on oxide junctions deposited by different methods on textured and planar surfaces, Phys. Status Solidi Appl. Mater. Sci. 214 (2017) 170, https://doi.org/10.1002/pssa.201700058.

[9] U. Römer, R. Peibst, T. Ohrdes, B. Lim, J. Krügener, E. Bugiel, et al., Recombination behavior and contact resistance of n+ and p+ poly-crystalline Si/mono-crystalline Si junctions, Sol. Energy Mater. Sol. Cells 131 (2014) 85–91, https://doi.org/10.1016/j.solmat.2014.06.003.

[10] M. Lozac'h, S. Nunomura, H. Sai, K. Matsubara, Passivation property of ultrathin SiOx:H/a-Si:H stack layers for solar cell applications, Sol. Energy Mater. Sol. Cells 185 (2018) 8–15, https://doi.org/10.1016/j.solmat.2018.05.004.

[11] F. Feldmann, R. Müller, C. Reichel, M. Hermle, Ion implantation into amorphous Si layers to form carrier-selective contacts for Si solar cells, Phys. Status Solidi Rapid Res. Lett. 8 (2014) 767–770, https://doi.org/10.1002/pssr.201409312.

[12] F. Feldmann, M. Simon, M. Bivour, C. Reichel, M. Hermle, S.W. Glunz, Carrier-selective contacts for Si solar cells, Appl. Phys. Lett. 104 (2014), https://doi.org/10.1063/1.4875904.

[13] U. Römer, R. Peibst, T. Ohrdes, B. Lim, J. Krügener, T. Wietler, et al., Ion implantation for poly-Si passivated back-junction back-contacted solar cells, IEEE J. Photovoltaics 5 (2015) 507–514, https://doi.org/10.1109/JPHOTOV.2014.2382975.

[14] D.L. Young, W. Nemeth, V. Lasalvia, R. Reedy, S. Essig, N. Bateman, et al., Interdigitated Back Passivated Contact (IBPC) solar cells formed by ion implantation, IEEE J. Photovoltaics. 6 (2016) 41–47, https://doi.org/10.1109/JPHOTOV.2015.2483364.

[15] C. Reichel, F. Feldmann, R. Müller, R.C. Reedy, B.G. Lee, D.L. Young, et al., Tunnel oxide passivated contacts formed by ion implantation for applications in silicon solar cells, J. Appl. Phys. 118 (2015), https://doi.org/10.1063/1.4936223, 205701.

[16] D. Yan, A. Cuevas, J. Bullock, Y. Wan, C. Samundsett, Phosphorus-diffused polysilicon contacts for solar cells, Sol. Energy Mater. Sol. Cells 142 (2015) 75–82, https://doi.org/10.1016/j.solmat.2015.06.001.

[17] G. Nogay, J. Stuckelberger, P. Wyss, Q. Jeangros, C. Allebé, X. Niquille, et al., Silicon-Rich silicon carbide hole-selective rear contacts for crystalline-silicon-based solar cells, ACS Appl. Mater. Interfaces 8 (2016) 35660–35667, https://doi.org/10.1021/acsami.6b12714.

[18] J. Stuckelberger, G. Nogay, P. Wyss, Q. Jeangros, C. Allebé, F. Debrot, et al., Passivating electron contact based on highly crystalline nanostructured silicon oxide layers for silicon solar cells, Sol. Energy Mater. Sol. Cells 158 (2016) 2–10, https://doi.org/10.1016/j.solmat.2016.06.040.

[19] Y. Larionova, H. Schulte-Huxel, B. Min, S. Hartmann, M. Turcu, T. Kulge, et al., Screen-printed double-side contacted POLO-cells with ultra-thin poly-Si layers and different transparent conductive oxides, 36th eur. PV sol, Energy Conf. Exhib. (Marseille, Fr. (2019) 172–175.

[20] W. Liu, X. Yang, J. Kang, S. Li, L. Xu, S. Zhang, et al., Poly-silicon passivating contacts for silicon solar cells: interface passivation and carrier transport mechanism, ACS Appl. Energy Mater. (2019), https://doi.org/10.1021/acsaem.8b02149 acsaem.8b02149.

[21] J.D. Hylton, R. Kinderman, A.R. Burgers, W.C. Sinke, P.M.M. Bressers, Uniform pyramid formation on alkaline-etched polished monocrystalline (100) silicon wafers, Prog. Photovolt. Res. Appl. 4 (1996) 435–438, https://doi.org/10.1002/(SICI)1099-159X(199611/12)4:6<435::AID-PIP150>3.0.CO, 2-5.

[22] S.N. Granata, T. Bearda, F. Dross, I. Gordon, J. Poortmans, R. Mertens, Effect of an in-situ H2 plasma pretreatment on the minority carrier lifetime of a-Si:H(i) passivated crystalline silicon, Energy Procedia 27 (2012) 412–418, https://doi.org/10.1016/j.egypro.2012.07.086.

[23] L. Korte, M. Schmidt, Doping type and thickness dependence of band offsets at the amorphous/crystalline silicon heterojunction, J. Appl. Phys. 109 (2011), https://doi.org/10.1063/1.3559296.

[24] W. Henrion, M. Rebien, H. Angermann, A. Röseler, Spectroscopic investigations of hydrogen termination, oxide coverage, roughness, and surface state density of silicon during native oxidation in air, Appl. Surf. Sci. 202 (2002) 199–205, https://doi.org/10.1016/S0169-4332(02)00923-6.

[25] S. Nunomura, I. Sakata, K. Matsubara, Electronic properties of ultrathin hydrogenated amorphous silicon, APEX 10 (2017), 081401, https://doi.org/10.7567/APEX.10.081401.

[26] B. Terreault, Hydrogen blistering of silicon: progress in fundamental understanding, Phys. Status Solidi Appl. Mater. Sci. 204 (2007) 2129–2184, https://doi.org/10.1002/pssa.200622520.

[27] A. Morisset, R. Cabal, B. Grange, C. Marchat, J. Alvarez, M.-E. Gueunier-Farret, et al., Conductivity and surface passivation properties of boron-doped poly-silicon passivated contacts for c-Si solar cells, Phys. Status Solidi 1800603 (2018), https://doi.org/10.1002/pssa.201800603, 1800603.

[28] J.H. Stathis, E. Cartier, Atomic hydrogen reactions with Pb centers at the (100) Si/SiO2 interface, Phys. Rev. Lett. 72 (1994) 2745–2748, https://doi.org/10.1103/PhysRevLett.72.2745.

[29] M. Lozac'h, S. Nunomura, H. Umishio, T. Matsui, K. Matsubara, Roles of hydrogen atoms in p-type poly-Si/SiOx passivation layer for crystalline silicon solar cell applications, Jpn. J. Appl. Phys. 58 (2019), 050915, https://doi.org/10.7567/1347-4065/ab14fe.

[30] S. Nunomura, H. Katayama, I. Yoshida, Hydrogen atom kinetics in capacitively coupled plasmas, Plasma Sources Sci. Technol. 26 (2017), 055018, https://doi.org/10.1088/1361-6595/aa6610.

[31] R.A. Sinton, A. Cuevas, Contactless determination of current–voltage characteristics and minority-carrier lifetimes in semiconductors from quasi-steady-state photoconductance data, Appl. Phys. Lett. 69 (1996) 2510–2512, https://doi.org/10.1063/1.117723.

[32] L. Tutsch, F. Feldmann, J. Polzin, C. Luderer, M. Bivour, A. Moldovan, et al., Solar Energy Materials and Solar Cells Implementing transparent conducting oxides by DC sputtering on ultrathin SiO x/poly-Si passivating contacts, Sol. Energy Mater. Sol. Cells 200 (2019), 109960, https://doi.org/10.1016/j.solmat.2019.109960.

[33] B. Demaurex, S. De Wolf, A. Descoeudres, Z. Charles Holman, C. Ballif, Damage at hydrogenated amorphous/crystalline silicon interfaces by indium tin oxide overlayer sputtering, Appl. Phys. Lett. 101 (2012), https://doi.org/10.1063/1.4764529.

[34] S. Nunomura, I. Sakata, K. Matsubara, Plasma-induced electronic defects: generation and annihilation kinetics in hydrogenated amorphous silicon, Phys. Rev. Appl. 10 (2018), 054006, https://doi.org/10.1103/PhysRevApplied.10.054006.

[35] G. Nogay, J. Stuckelberger, P. Wyss, E. Rucavado, C. Allebé, T. Koida, et al., Interplay of annealing temperature and doping in hole selective rear contacts based on silicon-rich silicon-carbide thin films, Sol. Energy Mater. Sol. Cells 173 (2017) 18–24, https://doi.org/10.1016/j.solmat.2017.06.039.

[36] R. Peibst, U. Römer, Y. Larionova, M. Rienäcker, A. Merkle, N. Folchert, et al., Working principle of carrier selective poly-Si/c-Si junctions: is tunnelling the whole story? Sol. Energy Mater. Sol. Cells 158 (2016) 60–67, https://doi.org/10.1016/j.solmat.2016.05.045.

[37] A. Descoeudres, Z.C. Holman, L. Barraud, S. Morel, S. De Wolf, C. Ballif, 21% efficient silicon heterojunction solar cells on n- and p-type wafers compared, IEEE J. Photovoltaics 3 (2013) 83–89, https://doi.org/10.1109/JPHOTOV.2012.2209407.

[38] R. Sinton, A. Cuevas, A quasi-steady-state open-circuit voltage method for solar cell characterization, in: 16th Eur. Photovolt. Sol. Energy Conf. (May 2000, Glas. UK), 2000, pp. 1–4, doi:citeulike-article-id:6901946.

[39] B. Sadigh, T.J. Lenosky, M.J. Caturla, A.A. Quong, L.X. Benedict, T. Diaz De La Rubia, et al., Large enhancement of boron solubility in silicon due to biaxial stress, Appl. Phys. Lett. 80 (2002) 4738–4740, https://doi.org/10.1063/1.1484557.

[40] D.E. Kane, R.M. Swanson, Measurement of the emitter saturation current by a contactless photoconductivity decay method (silicon solar cells), in: Proc. 18th IEEE Photovolt. Spec. Conf. Las Vegas, 1985, pp. 578–583.

[41] J. Melskens, B.W.H. van de Loo, B. Macco, L.E. Black, S. Smit, W.M.M. Kessels, Passivating contacts for crystalline silicon solar cells: from concepts and materials to prospects, IEEE J. Photovoltaics. 8 (2018) 373–388, https://doi.org/10.1109/JPHOTOV.2018.2797106.

[42] C. Battaglia, S.M. De Nicolás, S. De Wolf, X. Yin, M. Zheng, C. Ballif, et al., Silicon heterojunction solar cell with passivated hole selective MoO x contact, Appl. Phys. Lett. 104 (2014) 1–6, https://doi.org/10.1063/1.4868880.

[43] A.S. Grove, O. Leistiko, C.T. Sah, Redistribution of acceptor and donor impurities during thermal oxidation of silicon, J. Appl. Phys. 35 (1964) 2695–2701, https://doi.org/10.1063/1.1713825.
[44] M. Lehmann, N. Valle, J. Horzel, A. Pshenova, P. Wyss, M. Döbeli, et al., Analysis of hydrogen distribution and migration in fired passivating contacts (FPC), Sol. Energy Mater. Sol. Cells 200 (2019), https://doi.org/10.1016/j.solmat.2019.110018, 110018.
[45] M. Schnabel, B.W.H. Van De Loo, W. Nemeth, B. Macco, P. Stradins, W.M. M. Kessels, et al., Hydrogen passivation of poly-Si/SiOx contacts for Si solar cells using Al2O3 studied with deuterium, Appl. Phys. Lett. 112 (2018), https://doi.org/10.1063/1.5031118, 203901.